Polymer Nanostructures

DOI: 10.1002/anie.200901113

Nanocomposites with Structure Domains of 0.5 to 3 nm by Polymerization of Silicon Spiro Compounds**

Stefan Spange, Patrick Kempe, Andreas Seifert, Alexander A. Auer, Petra Ecorchard, Heinrich Lang, Meiken Falke, Michael Hietschold, Andreas Pohlers, Walter Hoyer, Gerhard Cox, Emanuel Kockrick, and Stefan Kaskel*

Dedicated to Professor Helmut Ringsdorf on the occasion of his 80th birthday

In recent years a variety of methods has been developed to produce organic–inorganic hybrid materials with defined nanostructures in the size range of 2 to 100 nm.[1] According to Sanchez and Ribot, these can be classified as type I and type II hybrids.[2] The latter have covalent bonds between their single phases, while type I composites do not. Literature methods for the production of nanostructured type I hybrid materials—for example, by the use of organic polymer templates—have a lower size barrier of 2–3 nm. Therefore, new synthetic concepts are required to develop nanostructures with dimensions of 0.5–2 nm. Such nanostructured hybrid materials are of high scientific and technical interest, for example, as potential precursors for highly porous oxides or organic polymer networks for gas storage. For this reason, this area is being intensively investigated worldwide.[1–13]

[*] Prof. Dr. S. Spange, P. Kempe, Dr. A. Seifert
Department of Polymer Chemistry
Chemnitz University of Technology
Strasse der Nationen 62, 09111 Chemnitz (Germany)
Fax: (+49) 371-531-21239
E-mail: stefan.spange@chemie.tu-chemnitz.de
Dr. A. A. Auer
Department of Theoretical Chemistry
Chemnitz University of Technology (Germany)
Dr. P. Ecorchard, Prof. Dr. H. Lang
Department of Inorganic Chemistry
Chemnitz University of Technology (Germany)
Dr. M. Falke, Prof. Dr. M. Hietschold
Department of Solid Surfaces Analysis
Chemnitz University of Technology (Germany)
Dr. A. Pohlers, Prof. Dr. W. Hoyer
Department of X-ray and Neutron Diffractometry
Chemnitz University of Technology (Germany)
Dr. G. Cox
Department of Polymer Physics
BASF SE, Ludwigshafen (Germany)
E. Kockrick, Prof. Dr. S. Kaskel
Department of Inorganic Chemistry I
Dresden University of Technology (Germany)

[**] We thank the DFG, BASF SE, and DAAD (project No D/07/09995) for financial support. We are grateful for the opportunity of using the UK superSTEM facility at the Daresbury laboratory funded by the EPSRC. We also thank Dr. M. Beiner (MLU Halle-Wittenberg) for SAXS measurements.

Supporting information for this article is available on the WWW under http://dx.doi.org/10.1002/anie.200901113.

Despite sophisticated techniques, the simultaneous polymerization of single monomers in one process leads to phase separation, whereby polymeric products with domains larger than 2–3 nm are always obtained. Therefore, polymerization methods are required which enable two different polymers to be made simultaneously from a single monomer. The previously known monomers for this purpose contain two building blocks suitable for polymerization.[14–17] Novak and co-workers used functionalized tetraalkoxysilanes for this so-called simultaneous polymerization, whereby two consecutive but independent chemical reactions, such as the sol–gel process with additional water and chain polymerization, afforded a nanocomposite.[14] This concept is extendable to titanium–oxopolyacrylate nanocomposites[18] and may also be applicable to other inorganic oxide/polymer nanocomposites. Well-defined aryl- or alkyl-bridged silanes or silsesquioxanes have been used to produce type II composites with dimensions of 0.5 to 2 nm.[19]

In the twin polymerization process—for example, by using tetrafurfuryloxysilane or several titanium monomers—inorganic and organic polymers are formed simultaneously in a single process, but with the concomitant formation of water.[15–17] Thus, the reproducible preparation of hybrid materials by the simultaneous formation of two structurally different, interpenetrating polymer structures in a single process step is a formidable scientific challenge.

The ring-opening polymerization of cyclic monomers with two different building blocks A and B can in principle yield two polymers, indicated as $(A)_n$ and $-(B)_n-$, without by-products. The envisaged monomer type $A(B)_x$ can possess a monocyclic, bicyclic (for example, spirobicyclic), or multicyclic structure with A at the center (Scheme 1). Two processes occur during the overall polymerization: the polymerization of $A(B)_x$ and the transformation of hybrid material type II to type I. Attractive forces and possible cross-

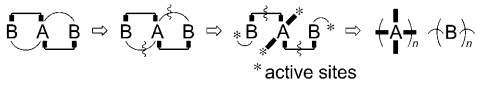

Scheme 1. The polymerization process starts from a spirocyclic compound with two organic groups B, each connected to the spirocenter A through two unequal bridging units. Both bridge types have different reactivities under the specific conditions of the bond-cleavage reaction. This leads to a consecutive bond cleavage of the two different bond types and, thus, two homopolymerizations take place before a complete separation occurs.

linking of $(A)_n$ and $-(B)_n-$ impede phase separation of $(A)_n$ and $-(B)_n-$ before the transformation is complete.

The novel polymerization process we introduce herein can be characterized as follows for the example of a spirobicyclic compound. Two molecular units (A and B) are combined to give a defined spirocyclic monomer with two groups B, which each have two unequal bridging units to the center A. The important point in this concept is the presence of two units (denoted as ∩ and ⊓) which have different reactivities, but are both capable of undergoing bond cleavage. The monomer type AB_2 in Scheme 1 corresponds to the spiro compound presented herein. If the cleavage of the A∩B bond is the first step, then a simultaneous formation of two different polymers, $-(A)_n-$ and $-(B)_n-$, is inherently allowed. However, as only the breaking of the A∩B bridge occurs, both polymer strands are linked to each other. Both polymers $-(A)_n-$ and $-(B)_n-$ are formed as condensation products only after the A⊓B bond is broken as well. This scenario is only possible due to the consecutive bond breaking of the two different bridging units A∩B and A⊓B, which impedes phase separation of freely mobile $(A)_n$ and $-(B)_n-$ strands during the polymerization process. Only if the breaking of the A⊓B bridge is complete do the two strands lie separately, but adjacent to one another. Therefore, a suitable monomer for the new type of polymerization should have two basic properties. It should 1) consist of different parts (A and B) that are precursors for the formation of polymers without generating perturbing by-products and 2) the parts A and B should be linked by two unequal bridge units, which can be cleaved under the same conditions but at different rates. Thus, a consecutive cleavage of the two different bridge types takes place.

A compound that fulfills the two important prerequisites for the new concept of polymerization is the previously unknown 2,2′-spirobi[4*H*-1,3,2-benzodioxasiline] (**1**). It is prepared by a fluoride-catalyzed transesterification of salicyl alcohol and tetramethoxysilane (see the Supporting Information). The molecular solid-state structure of the chiral compound **1** was proved by single-crystal X-ray structure analysis (Figure 1).

The (theoretical) overall equation for the polymerization of **1** gives SiO_2 and a linear phenolic resin without by-products (Scheme 2). The two different types of Si-O-C bonds (as asymmetric bridges) can be readily cleaved by acid or base catalysis.

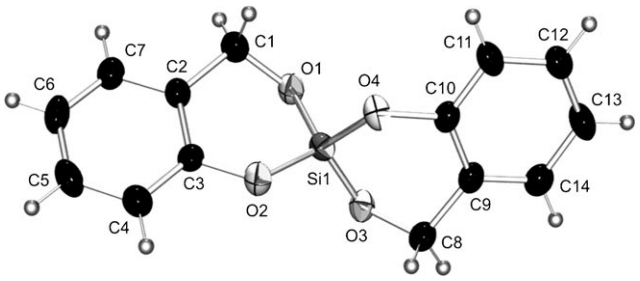

Figure 1. Molecular solid-state structure (50% probability level) of **1**. The racemic mixture of **1** crystallizes in the monoclinic centrosymmetric space group $P2_1/n$ with $a = 13.6917(7)$, $b = 5.8780(2)$, $c = 15.7413(8)$ Å, $\beta = 106.201(5)°$, and $V = 1216.55(10)$ Å^3 (for further details see the Supporting Information).

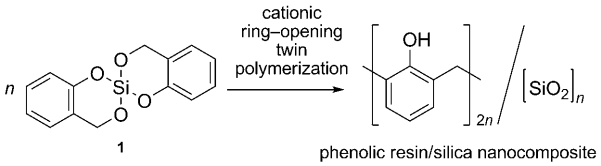

Scheme 2. The (theoretical) overall equation for the cationic polymerization of **1** gives SiO_2 and a linear phenolic resin (presented here: *ortho–ortho′* substitution) without by-products.

The addition of water as a proton source is not necessary to produce the inorganic oxide phase. In contrast to those processes occurring in aqueous solution, the proton sources for the silica surface structure are the aromatic protons in the *ortho* and *para* positions. The phenolic resin is formed by an electrophilic aromatic substitution reaction which takes place under non-aqueous conditions. This is an important difference compared to the strategy developed by Novak and coworkers.[14] Furthermore, the polymerization mechanism of our process is completely different.

The phenolic resin/silica composites previously described in the literature are generally prepared by sol–gel-assisted polycondensation of phenol and formaldehyde.[20–22]

Quantum chemical calculations further confirm that monomer **1** possesses the required properties for asymmetric ring-opening under acid catalysis. The initiating step of the polymerization is the addition of a proton at one of the two types of non-equivalent oxygen atoms of **1**, thereby resulting in two structural isomers (**1**-$\mathbf{H}^+$). Calculations of the protonation energy and charge analysis indicate that the oxygen atoms do not differ significantly in their basicity (Figure 2). However, the ring-opening reaction of **1**-$\mathbf{H}^+$ clearly gives the *ortho*-siloxy-substituted benzylium ion (**1**-$\mathbf{CH_2}^+$; Figure 2) after protonation at the oxygen atom of the oxymethylene group. The reason that this occurs is the possibility for delocalization of the positive charge, as can be seen from the electrostatic potential (Figure 2, bottom right). The formation of the phenolic resin moiety can be attributed to consecutive electrophilic substitution reactions of **1**-$\mathbf{CH_2}^+$ with **1**, which regenerate the proton (Figure 3, structures A, B, and D).

The results of the electronic structure calculations indicate that this reaction is associated with a comparably low energy barrier. Successive proton transfer ultimately leads to a structure in which the proton is located in the center of the product species and stabilized by hydrogen bonding (Figure 3, structure D). The formation of a silica network from the same reactants A proceeds through proton transfer, which leads to the formation of a siloxane bridge and a phenol group (Figure 3, structure C). This reaction path, in principle, competes with the electrophilic substitution mentioned above. However, the energy barrier is significantly higher, as the silanol reactant has to penetrate the negative charge density of the oxygen atoms to pass through the transition state. After the formation of a dimer, either by linking through a methylene bridge or by the formation of a siloxane group, several reaction paths open up—ranging from successive polymerization to yield the phenolic resin to the rich variety of reactions that form the silica network. The mechanisms are related to the typical reaction paths known

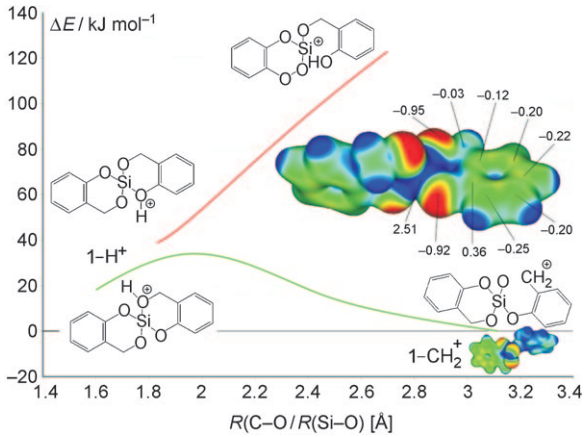

Figure 2. Potential energy curves for the ring-opening reaction of the protonated species of **1**. Red curve: Protonation at the oxygen atom of the Si-O-aryl group and ring opening by cleavage of the silicon–oxygen bond. Green curve: Protonation at the oxygen atom of the Si-O-CH_2-aryl group and ring opening by cleavage of the methylene–oxygen bond. Center right: Electrostatic potential and natural bond orbital (NBO) atomic charges of selected atoms of **1**. Bottom right: Electrostatic potential of the equilibrium structure after proton-induced ring opening. Red and blue indicate regions of high and low charge density, respectively.

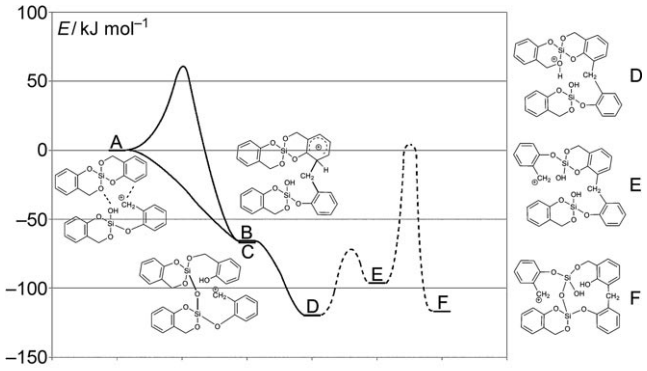

Figure 3. Potential energy curves in the formation of a dimer from **1**-CH_2^+ and **1** as calculated by density functional theory (B3-LYP/TZVP). Pathways to the formation of the phenolic resin are marked in gray (lower curve, A→C→D→E), formation of siloxane bridges are marked in black (upper curve, A→B and E→F). The two dashed curves denote likely reaction pathways among a multitude of possible reactions.

from sol–gel processes, although the structural circumstances are unique in this case. Figure 3 gives an overview of the possible steps.

Theoretical calculations show that formation of the phenolic resin is kinetically favored, as the formation of a siloxane bridge is associated with a comparably high energy barrier at any point during the reaction. This is supported by preliminary ^{1}H NMR studies (see the Supporting Information).

Both of the cationically active dimeric species B and C are key intermediates to form either silica or phenolic resin chains. Importantly, B and C have nearly the same thermodynamic stability (see Figure 3), but the formation of B occurs faster. This is the basis for the simultaneous formation of two different polymers which are covalently linked and are preferentially formed consecutively by the same catalytic process (protonation reaction) at higher temperature. The proposed mechanism also gives an explanation for the mutation of type II to type I hybrid material. A more detailed description of the mechanism, the intermediates, and structure–property relationships are topics for further research.

For our study, polymerizations of **1** were performed in the melt at 85 °C and in solution at 25 °C. The use of trifluoroacetic acid ($pK_a = 0.25$) as the catalyst afforded a transparent monolith (Figure 4 A, see also the Supporting Information). Monomer **1** undergoes complete conversion, as shown by the solid-state NMR spectra of the composite product: The ^{29}Si NMR spectra of monomer **1** shows one sharp signal, whereas the composite material shows only signals of a silica-like

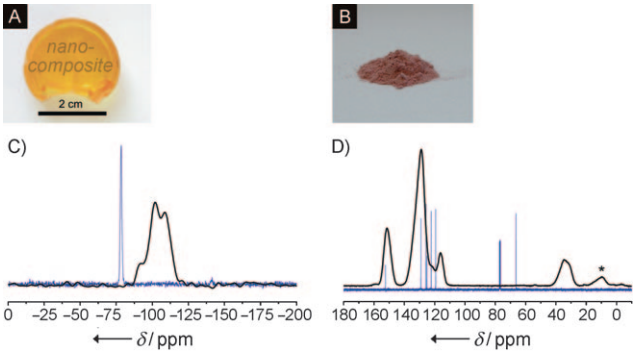

Figure 4. Phenolic resin/silica nanocomposites are obtained by cationic ring-opening twin polymerization of **1**. A) Transparent monolithic phenolic resin/silica nanocomposite obtained with trifluoroacetic acid as catalyst (**1**/CF_3CO_2H = 25:1; 4 h in the melt at 85 °C). B) Solid material formed after initiation with methanesulfonic acid (**1**/CH_3SO_3H = 25:1, solution in CH_2Cl_2, 0 °C). C) Solid-state ^{29}Si-{^{1}H}-CP-MAS NMR spectra of **1** (blue line) shows a signal at $\delta = -78.4$ ppm. After polymerization, the Q_2 ($\delta = -102$ ppm), Q_3 ($\delta = -92$ ppm), and Q_4 signals ($\delta = -109$ ppm) of silica are obtained (black line, quantitative ^{29}Si-{^{1}H}-MAS NMR). D) ^{13}C NMR spectrum indicating the formation of a phenolic resin (blue line: ^{13}C-{^{1}H} NMR of **1** dissolved in $CDCl_3$; black line: ^{13}C-{^{1}H}-CP-MAS NMR of the composite material). The asterisk (*) indicates a spinning side band.

structure (Figure 4 C). The polymerization reaction rate increases drastically when methanesulfonic acid ($pK_a = -2.0$) is used as the catalyst. In this case, the polymerization was carried out in dichloromethane solution, which led to precipitation of the phenolic resin/silica nanocomposite (Figure 4 B). A detailed description of the experiments is given in the Supporting Information. The ^{13}C and ^{29}Si solid-state NMR spectra of the precipitate and the monolithic products do not show any significant differences, thus indicating that the same molecular structure is obtained, irrespective of the synthetic procedure used. The $Q_{2/3}$ signals correspond to the generated silanol units or intact Si-O-aryl groups. The quantitative ratio of the $(Q_2 + Q_3)/Q_4$ signals determined by fitting calculations is close to 1, which indicates a low-condensed silica phase. The stoichiometry of the SiO_2 phase is, as expected, between that of pure SiO_2 (fully condensed) and $SiO_{1.5}(OH)$ (surface Si atoms as Si-OH

groups; for example, cubic octasilicic acid). About 50% of the silicon atoms are found at the interface with the phenolic resin component, either as Si-O-aryl or as Si-OH and $Si(OH)_2$ groups. The solid-state ^{13}C-{^1H}-CP-MAS NMR spectra of the monolithic products clearly show the formation of a phenolic resin (Figure 4D). Each step in the polycondensation reaction of **1**-$\mathbf{H}^+$ with **1** generates only one proton, which originates from the aromatic ring at the formerly unsubstituted *ortho* or *para* position. As a result, the proton generated is either the source of a silanol or a phenolic OH group. Overall, there are not enough protons available to produce such large amounts of phenolic OH groups and silanols simultaneously, as would be expected from the sum of the Q_2 and Q_3 NMR signals. This might be interpreted as an indication of remaining Si-O-aryl bridges in the hybrid material, and is another confirmation of the polymerization mechanism proposed on the basis of the quantum chemical studies.

Transmission electron microscopy (TEM) studies have been carried out to obtain more detailed information about the local Si distribution in the monolithic phenolic resin/silica nanocomposite material. Thin slices of material were prepared by ultramicrotomy. Standard bright-field TEM images do not show any strong variations in the contrast, thus indicating a homogeneous Si distribution without any Si agglomerates down to the sub-micrometer range. This was further confirmed by local energy-disperive X-ray spectroscopy (EDX) measurements of the carbon, oxygen, and silicon concentrations. High-resolution TEM images only show the typical phase contrast of an amorphous sample (for WAXS/SAXS analyses see the Supporting Information). Very thin areas at the edge of the microtome-sectioned slices were imaged by high-angle annular dark-field (HAADF) scanning TEM and energy-filtered TEM (EFTEM). The size of the electron spot in the HAADF STEM images was set below 1 nm. The high-resolution contrast images show bright clusters in ranges smaller than 2–3 nm. The structure sizes correlate with the magnifications used (see Figure 5A and B). The HAADF signal for the composite samples increases monotonically with the atomic number of the scattering elements; thus, the clusters in the HAADF images represent Si-rich areas (see also the Supporting Information). This was confirmed by the elemental distribution images of C, O, and Si using EFTEM (Figure 5C–E). All three images show a granular structure on the nanometer scale with similar feature sizes, but different distribution. The Si image (Figure 5E) shows 2–3 nm large clusters within the nanocomposite material, which agrees well with the HAADF data.

In some thin sample areas, Si image features (Figure 5E, marked by arrows) which are dark, appear bright in the carbon image (Figure 5C). Furthermore, dark Si features appear less dark in the O image, thus confirming that oxygen is present not only in the silica nanostructures, but also in the phenolic resin. A change in the specimen through electron beam impact over the course of the whole measurement cannot be excluded. The high-resolution TEM, HAADF-STEM, and EFTEM measurements prove that the size of the structure domains of the phenolic resin and silica components in the hybrid material are less than 3 nm and that no larger domains are formed by either of the components in the whole monolith.

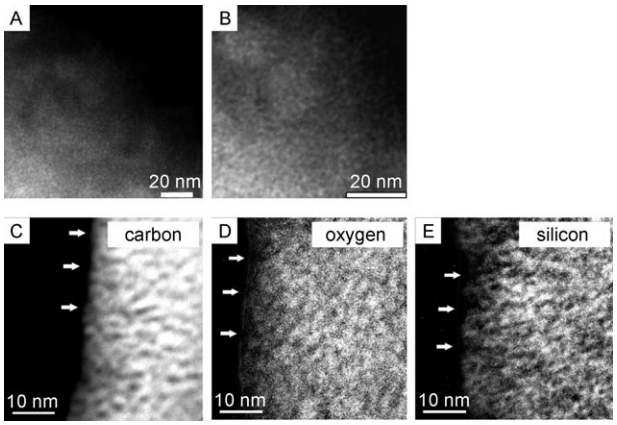

Figure 5. A,B) HAADF-STEM images at different magnifications from the edge of a thin section of the composite material. C–E) EFTEM images of the phenolic resin/silica nanocomposite with the elemental distribution of carbon (C), oxygen (D), and silicon (E). The arrows show the same positions.

Highly porous carbon can be obtained from the composite after carbonizing the nanocomposite to a carbon/silica nanocomposite followed by removal of the silica phase using hydrofluoric acid. On the other hand, highly porous silica is obtained by direct oxidation of the composite or by oxidizing the carbon/silica composite. The porous silica and carbon material represent the complementary phases of the original composite. The results of further investigations (determination of pore sizes and size distributions) allow for estimates on the dimensions of the composite nanostructures and confirm the dimensions of the nanostructures determined using electron microscopy (Figures 6C, D). Aberration-corrected HAADF imaging was carried out at 0.1 nm resolution to show the nanometer-scale porosity of the silica product after oxidation at 900 °C. Figure 6E shows the HAADF images at two different magnifications. The low-magnification image on the left reveals the porous sample structure, with bigger pores and fine pores similar to the Si distribution shown for the composite determined by EFTEM.

The nanoporous structure on the nanometer scale is revealed in the magnified image of Figure 6E. Furthermore, a bright 2 nm silica cluster is visible in the upper right corner. The HAADF data proves that the final oxidized silica product also retains its nanoporosity (see also the Supporting Information). Investigations on the porous silica and carbon materials that can be obtained by treatment of the hybrid material yield further information on the nanostructure of the original composite, thereby confirming the finding that the new material is indeed composed of silica and phenolic resin structures of 0.5 to 2 nm size.

In conclusion, the cationic polymerization of a silicon spiro compound containing phenolic resin and silica monomeric building blocks presented herein leads to highly nanostructured, amorphous hybrid materials in a single process step. The key feature of this process is that two different macromolecular structures can be formed in a single process without by-products. Both of the created polymers

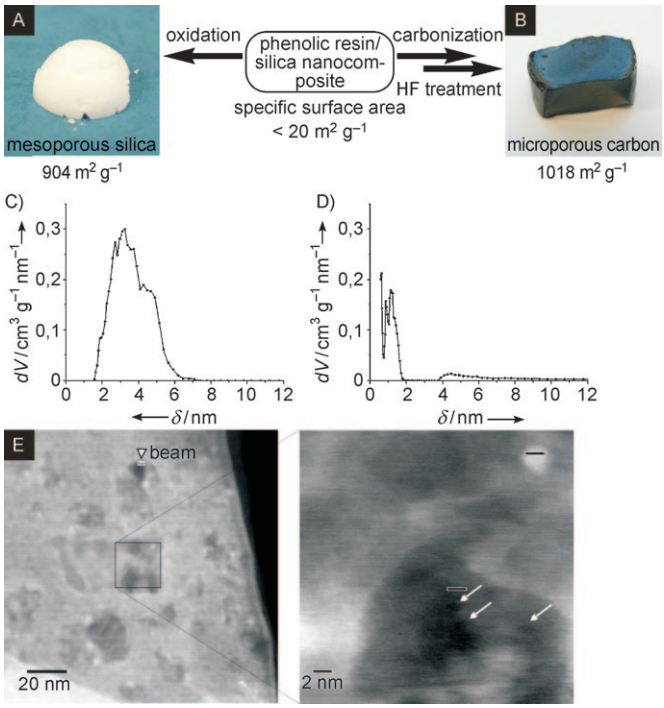

Figure 6. Transformation of phenolic resin/silica nanocomposites to pure porous silica or carbon phases. A) Oxidation to monolithic silica with a high specific surface area of 904 $m^2 g^{-1}$ (at 900 °C in air). B) Microporous monolithic carbon (1018 $m^2 g^{-1}$) can be obtained after carbonization at 800 °C under argon followed by treatment with HF. C) Pore-size distribution (DFT method) of the monolithic silica (see the Supporting Information). D) Pore-size distribution (DFT method) of the microporous carbon (see the Supporting Information). E) HAADF images of the silica sample oxidized at 900 °C (0.1 nm probe size in an aberration corrected STEM). The silica appears bright, pores appear dark.

can independently form linear, branched, or cross-linked structures, depending on the number of functionalities of the components built into the monomer. The nanostructures reach down to the molecular dimensions of single polymer chains, as demonstrated by TEM and porosity texture. As the polymerization process can occur without solvents and without the formation of by-products, it offers a completely new perspective on the development of nanocomposites and monolithic porous materials. The new process is very easy to perform technically, as the monomers are readily available. In general, the process can be applied to an almost infinite number of other molecular structures by substitution of the central atom (here silicon) and the phenol resin block. By careful choice of the monomer and reaction conditions, novel nanocomposites can be formed with designed chemical composition and material properties.

Received: February 26, 2009
Revised: July 27, 2009
Published online: September 25, 2009

Keywords: cationic polymerization · microporous materials · nanostructures · organic–inorganic hybrid composites · spiro compounds

[1] G. Kickelbick, *Hybrid Materials—Synthesis Characterization, and Applications*, Wiley-VCH, Weinheim, **2007**.
[2] C. Sanchez, F. Ribot, *New J. Chem.* **1994**, *18*, 1007–1047.
[3] K. P. Gierszal, M. Jaroniec, *J. Am. Chem. Soc.* **2006**, *128*, 10026–10027.
[4] M. E. Davis, *Nature* **2002**, *417*, 813–821.
[5] Z. Wang, A. Stein, *Chem. Mater.* **2008**, *20*, 1029–1040.
[6] M. Jaroniec, J. Choma, J. Gorka, A. Zawislak, *Chem. Mater.* **2008**, *20*, 1069–1075.
[7] M. Choi, R. Ryoo, *Nat. Mater.* **2003**, *2*, 473–476.
[8] a) A. Thomas, F. Goettmann, M. Antonietti, *Chem. Mater.* **2008**, *20*, 738–755; b) Y.-S. Hu, R. Demir-Cakan, M.-M. Titirici, J.-O. Müller, R. Schlögl, M. Antonietti, J. Maier, *Angew. Chem.* **2008**, *120*, 1669–1673; *Angew. Chem. Int. Ed.* **2008**, *47*, 1645–1649.
[9] S. H. Joo, S. J. Choi, I. Oh, J. Kwak, Z. Liu, O. Terasaki, R. Ryoo, *Nature* **2001**, *412*, 169–172.
[10] F. Schüth, *Angew. Chem.* **2003**, *115*, 3730–3750; *Angew. Chem. Int. Ed.* **2003**, *42*, 3604–3622.
[11] C. T. Kresge, M. E. Leonowicz, W. J. Roth, J. C. Vartuli, J. S. Beck, *Nature* **1992**, *359*, 710–712.
[12] J. S. Beck, J. C. Vartuli, W. J. Roth, M. E. Leonowicz, C. T. Kresge, K. D. Schmitt, C. T. W. Chu, D. H. Olson, E. W. Sheppard, S. B. McCullen, J. B. Higgins, J. L. Schlenker, *J. Am. Chem. Soc.* **1992**, *114*, 10834–10843.
[13] N. K. Raman, M. T. Anderson, C. J. Brinker, *Chem. Mater.* **1996**, *8*, 1682–1701.
[14] a) M. W. Ellsworth, B. M. Novak, *J. Am. Chem. Soc.* **1991**, *113*, 2756–2758; b) B. M. Novak, C. Davies, *Macromolecules* **1991**, *24*, 5481–5483; c) B. M. Novak, *Adv. Mater.* **1993**, *5*, 422–433; d) M. W. Ellsworth, B. M. Novak, *Chem. Mater.* **1993**, *5*, 839–844; e) B. M. Novak, M. W. Ellsworth, C. Verrier, *ACS Symp. Ser.* **1995**, *585*, 86–96.
[15] S. Grund, P. Kempe, G. Baumann, A. Seifert, S. Spange, *Angew. Chem.* **2007**, *119*, 636–640; *Angew. Chem. Int. Ed.* **2007**, *46*, 628–632.
[16] A. Mehner, T. Rüffer, H. Lang, A. Pohlers, W. Hoyer, S. Spange, *Adv. Mater.* **2008**, *20*, 4113–4117.
[17] S. Spange, S. Grund, *Adv. Mater.* **2009**, *21*, 2111–2116.
[18] O. Kameneva, A. I. Kuznestov, L. A. Smirnova, L. Rozes, C. Sanchez, A. Alexandrov, N. Bityurin, K. Chhor, A. Kanaev, *J. Mater. Chem.* **2005**, *15*, 3380–3383.
[19] a) K. J. Shea, O. Webster, D. A. Loy, *Mater. Res. Soc. Symp. Proc.* **1990**, *180*, 975–980; b) K. J. Shea, D. A. Loy, O. W. Webster, *Chem. Mater.* **1989**, *1*, 572–574; c) K. J. Shea, D. A. Loy, O. Webster, *J. Am. Chem. Soc.* **1992**, *114*, 6700–6710; d) K. J. Shea, D. A. Loy, *Chem. Mater.* **2001**, *13*, 3306–3319.
[20] K. Haraguchi, Y. Usami, K. Yamamura, S. Matsumoto, *Polymer* **1998**, *39*, 6243–6250.
[21] J. M. Lin, C. C. M. Ma, F. Y. Wang, H. D. Wu, S. C. Kuang, *J. Polym. Sci. Part B* **2000**, *38*, 1699–1706.
[22] a) G. Hernández-Padrón, R. M. Lima, R. Nava, M. V. García-Garduño, V. M. Castaño, *Adv. Polym. Technol.* **2002**, *21*, 116–124; b) G. Hernández-Padrón, F. Rojas, M. García-Garduño, M. A. Canseco, V. M. Castaño, *Mater. Sci. Eng. A* **2003**, *355*, 338–347; c) G. Hernández-Padrón, F. Rojas, V. M. Castaño, *Nanotechnology* **2004**, *15*, 98–103.

